

Mode-space energy distribution in instability-driven plasma turbulence

P. W. Terry, K. D. Makwana, M. J. Pueschel, D. R. Hatch, F. Jenko, and F. Merz

Citation: *Physics of Plasmas* (1994-present) **21**, 122303 (2014); doi: 10.1063/1.4903207

View online: <http://dx.doi.org/10.1063/1.4903207>

View Table of Contents: <http://scitation.aip.org/content/aip/journal/pop/21/12?ver=pdfcov>

Published by the [AIP Publishing](#)

Articles you may be interested in

[Regulation of electron temperature gradient turbulence by zonal flows driven by trapped electron modes](#)

Phys. Plasmas **21**, 052306 (2014); 10.1063/1.4875740

[Impurity transport in trapped electron mode driven turbulence](#)

Phys. Plasmas **20**, 032310 (2013); 10.1063/1.4796196

[Studies of turbulence and transport in Alcator C-Mod H-mode plasmas with phase contrast imaging and comparisons with GYRO](#)

Phys. Plasmas **16**, 012502 (2009); 10.1063/1.3057420

[Electromagnetic turbulence driven by the mixed mode instability](#)

Phys. Plasmas **15**, 094503 (2008); 10.1063/1.2985776

[Nonlocal theory and turbulence of the sheath-driven electron temperature gradient instability](#)

Phys. Plasmas **8**, 750 (2001); 10.1063/1.1343513

A collection of five pieces of industrial vacuum equipment from Pfeiffer Vacuum. From top-left to bottom-right: a red rectangular turbopump, a cylindrical stainless steel turbopump, a white rectangular turbopump, a red cylindrical turbopump with a long metal shaft, and a large, complex stainless steel chamber or component.

 Vacuum Solutions from a Single Source

- Turbopumps
- Backing pumps
- Leak detectors
- Measurement and analysis equipment
- Chambers and components

PFEIFFER  **VACUUM**

Mode-space energy distribution in instability-driven plasma turbulence

P. W. Terry,¹ K. D. Makwana,¹ M. J. Pueschel,¹ D. R. Hatch,² F. Jenko,^{3,a)} and F. Merz³

¹University of Wisconsin-Madison, Madison, Wisconsin 53706, USA

²University of Texas at Austin, Austin, Texas 78712, USA

³Max-Planck-Institut für Plasmaphysik, 85748 Garching, Germany

(Received 24 September 2014; accepted 16 November 2014; published online 4 December 2014)

Energy transfer to damped modes in gyrokinetic ion temperature gradient driven turbulence is studied to understand the transfer dynamics and find scaling representations for the heavily populated mode space. Proper orthogonal and linear eigenmode decompositions are introduced and examined to assess whether modes are well-resolved and what scales they encompass. It is observed that damped modes across a range of inhomogeneous scales receive energy simultaneously and directly from the unstable mode, constituting a form of parallel transfer, distinct from the serial mode-to-mode transfer of the wavenumber cascade of hydrodynamic turbulence. Controlling for modes that are well resolved and labeling the modes of the linear decomposition in order of damping rate, energy transfer in the mode space satisfies an equipartition of the energy dissipation rate, leading to a simple rule for the distribution of energy in the space of damped modes. Energy dissipation rate equipartition is the form that the canonical nonlinear invariance of energy transfer assumes in a dissipation range with parallel rather than serial transfer. © 2014 AIP Publishing LLC.

[<http://dx.doi.org/10.1063/1.4903207>]

I. INTRODUCTION

In hydrodynamic turbulence of a homogeneous unbounded medium, the distribution of energy in wavenumber space is governed by a set of simple but powerful principles. When the advective nonlinearity dominates dissipation, a condition associated with the inertial range of scales, the nonlinearity produces universal behavior. Energy is carried from large scale to small scale in a cascade, a serial progression through ever smaller scales via a sequence of quasi-local steps. The cascade is self similar with scale, so that the energy transfer rate, energy dissipation rate, and structure functions are scale invariant in the inertial range. This leads to power-law distributions for these quantities,^{1–3} for which spectral indices bear a direct relationship with the form of the nonlinearity.

It has long been assumed that instability-driven plasma turbulence can be described, at least qualitatively, in an analogous fashion.⁴ To wit, instability replaces stirring but is otherwise localized to a range of scales that are sufficiently large to make collisional dissipation weak compared to the rate at which energy is released from equilibrium gradients by the instability. Energy is transferred by advective nonlinearities to small scales where it is dissipated by collisional processes. Recently, it has been shown that instability-driven plasma turbulence deviates strikingly from this picture.⁵ Consider flux tube representations⁶ of gyrokinetic plasma turbulence. The standard notion of energy transfer to small dissipated scales in the x and y directions perpendicular to the equilibrium magnetic field remains operative.⁷ However, there is strong damping in the form of turbulent energy sinks at the same large scales that support instability. This

dissipation arises from nonlinear energy transfer in a dissipative space of independent coordinates that exists because bounded plasmas have degrees of freedom rendered unsuitable to wavenumber representation by inhomogeneity. These degrees of freedom encompass the extended ballooning angle θ of real space, which combines the coordinate parallel to the background magnetic field with the radial wavenumber,⁸ and the two velocity space directions v_{\parallel} and μ , where μ is the magnetic moment. These degrees of freedom are spanned by modes that are excited by nonlinear mode coupling at the same perpendicular scales as the instability. Provided collisionality remains above some small threshold value,⁹ a condition satisfied in most present-day devices,¹⁰ these modes introduce significant large scale damping. In fluid models, a similar situation arises.^{11,12} In addition to any inhomogeneity in ordinary space, which leads to a spectrum of eigenmodes, a finite set of moment equations replaces velocity space, yielding a discrete set of n eigenmodes, where n is the number of independent dynamical fields retained in the fluid closure.¹³ If m is the number of modes spanning inhomogeneous directions, the total number of modes is $n \times m$.

In initial value treatments of instability-driven turbulence, damped modes are invisible, despite receiving energy in a robust nonlinear transfer process, unless the turbulence is subjected to mode decomposition analysis.¹⁴ For gyrokinetic models, the number of damped modes that play a role in instability saturation and nonlinear dynamics is extremely large. Consequently, the prompt effect of instability is an apportionment of energy across a heavily populated, dissipated *mode space*. While energy transfer in perpendicular scales is present, it is subject to dissipation at all perpendicular scales, with dissipation peaking in the region of instability,⁵ and dissipation rates that can exceed energy transfer rates to perpendicular scales by as much as an order of

^{a)}Present address: Department of Physics and Astronomy, University of California at Los Angeles, Los Angeles, California 90095, USA.

magnitude.¹⁵ The dissipation rate at large scales is intrinsically nonlinear. It depends on the rate of energy transfer to the mode space of the inhomogeneous degrees of freedom and the energy distribution of these modes. Understanding this transfer and the energy distribution of these modes is key to quantifying the dissipation, understanding the saturation, and ultimately deriving physics-based models for experimentally important quantities such as saturation levels, spectra, and transport. Because the mode space is dissipated, the standard formulations of universality and scaling from inertial range hydrodynamic turbulence would not be expected to govern the energy distribution.

In this paper, we investigate the distribution of energy and the energy dissipation rate in the dissipated mode space of the gyrokinetic distribution function for numerical solutions of ion temperature gradient (ITG) turbulence. ITG turbulence is a primary cause of anomalous transport in magnetic confinement devices.¹⁶ The shear number of modes excited in numerical simulation— $O(10^4)$ for typical present-day resolutions—could produce a state with a high degree of complexity and corresponding complexities in its characterization. On the other hand, the large numbers may permit a statistical characterization with some order, possibly imposed by the nonlinearity. In particular, we are interested in the possibility that the large number of accessible modes might, under appropriate coupling, confer equal access to the energy of the instability, giving rise to some form of energy equipartition. The object of this investigation is to determine the form of the energy distribution in mode space, to determine if its form reflects underlying physical properties from which the shape can be predicted, and if so, what those properties are. If the distribution can be characterized in a fairly simple way, it means that energy dissipation can also be characterized, allowing for a quantitative understanding of saturation by the damped modes.

From the outset, the objectives just stated cause us to seek a mode labeling construct that treats the space as *unitary*, and therefore utilizes a single mode index. The alternative is to use some form of basis functions for each of the three directions θ , v_{\parallel} , and μ , with corresponding indices for each dimension. Because the system is anisotropic in this space, three sets of indices would make it difficult to detect underlying, unitary structure, should it be present. There is precedent for such single-index labeling, as it emerges naturally in optimal decomposition schemes such as proper orthogonal decomposition (POD) and singular value decomposition.¹⁷ However, we will demonstrate that it can also be implemented with linear eigenmodes.

To accomplish our objectives, it is necessary to examine mode decompositions and characterize energy pathways before proceeding to investigate the mode-space energy distribution. The mode decomposition used to represent fluctuations in the inhomogeneous directions θ , v_{\parallel} , and μ affects the mode space energy distribution. There is no unique decomposition, and thus the question of the most appropriate decomposition arises. In previous studies, proper orthogonal decomposition, chosen for its decomposition of energy with the fewest modes, has been the principal probe of damped-mode activity in gyrokinetic turbulence. However, in the

wavenumber range of interest, where both the growth rate and the damping rate associated with stable modes peaks, linear rates of growth and damping exceed nonlinear energy transfer rates to large perpendicular wavenumbers. This situation is favorable for a mode decomposition constructed from the eigenmodes of the linear gyrokinetic operator. Projections of the turbulent gyrokinetic distribution onto linear eigenmodes have tended to produce large amplitudes that are not representative of their importance to the dynamics.¹⁸ This leads us to investigate when the components of a mode decomposition are well resolved, and therefore capable of rendering a physically meaningful expansion of the distribution function. We introduce a metric for mode resolution that gives a quantitative measure of when the decomposition of the energy distribution is meaningful. Using our metric for mode resolution, we determine the number of modes that are properly resolved for POD and the linear eigenmode decomposition. From Fourier transforms of the decomposed gyrokinetic distribution, we also determine how mode number varies with scale, and therefore the range of scales captured by the well resolved modes.

To understand energy transfer in mode space, it is instructive to characterize the energy pathway. Over the range of well resolved modes, the pathway is *parallel*, proceeding directly and simultaneously from the unstable mode to all well resolved damped modes. This behavior is measured quantitatively from the response of each damped mode to an instantaneous energy increment in the unstable mode. The response time is independent of mode number for both the POD and the linear eigenmode decomposition.

Provided appropriate representations are employed, energy transfer in mode-space is found to have underlying order that is reflected in the energy distribution shape. When the well-resolved modes of the linear eigenmode decomposition are labeled in order according to the magnitude of their damping rate, the energy dissipation rate distribution is found to be roughly constant over the first 1200 of these modes. This latent behavior is consistent with a power-law energy distribution that has the damping rate as the scale variable, analogous to the wavenumber in hydrodynamic turbulence. It applies here in a dissipation range because the energy transfer is parallel. Each mode receives energy directly from the nonlinearity at a nonlinear rate, not subject to the cascading loss of a serial cascade.

The remainder of the paper is organized as follows. Section II contains a brief description of the gyrokinetic equation and its phase space, followed by an examination of mode space decompositions. In Sec. III, we present a qualitative description of energy transfer in this space resulting from a perturbation of the energy of the unstable mode. In Sec. IV, we introduce a construct for a scalable description of energy transfer in mode space. Using it, we examine energy distributions and underlying physical meaning. Section V contains a discussion of the results and conclusions.

II. MODE DECOMPOSITION STUDIES

The linear eigenmode decomposition offers a transparent connection to linear physics. This is advantageous in

regimes where linear physics dominates the nonlinearity. However, the linear decomposition can be at a disadvantage relative to the POD if mode energies do not decrease significantly across a sample associated with a truncation. An optimal decrease is assured for POD, by construct.¹⁷ When the decrease is slight for a sample of linear eigenmodes, the sample may not be properly resolving the physics. In light of these issues, this section examines the POD and linear eigenmode decompositions and their representation of fluctuations. We consider whether a given mode in the decomposition is properly resolved, what range of spatial scales is captured by the set of properly resolved modes, and whether energy decreases over the set. We also consider how the size of hyper diffusion coefficients affects these properties.

A. Mode decompositions

We begin by discussing briefly the two mode decompositions studied here, both of which are decompositions of the gyrokinetic distribution function. This distribution function is defined on a five-dimensional phase space.¹⁹ In toroidal flux-tube representations,⁶ a Fourier transform in x and y yields the perpendicular wavenumbers k_x and k_y . An infinite expansion in eigenmodes, each of which is a parametric function of k_x and k_y , spans the remaining three inhomogeneous directions of phase space, corresponding to ballooning angle θ , parallel velocity v_{\parallel} , and magnetic moment μ . Discretization truncates the expansion to $N = n_{\theta} \times n_{v_{\parallel}} \times n_{\mu}$ eigenmodes, where the n 's are the number of grid points in each direction. For the parameters of the Cyclone base case (CBC),²⁰ there is a single unstable linear eigenmode for each wavevector (k_x, k_y) in the unstable range; the remaining eigenmodes are stable. The joint space of perpendicular wavenumbers and damped eigenmodes can be visualized as a series of nonlinearly coupled k_x - k_y planes, one for each eigenmode (see Fig. 1 of Ref. 14). A single wavenumber triplet, for example, one in which wavenumbers k and $k - k'$ on the plane of the instability beat with a third wavenumber k' on each of the damped-mode planes,¹¹ simultaneously accesses thousands of stable modes. Because nonlinear coupling of the unstable mode to the damped modes involves the same wavenumber pair k and $k - k'$ of large-amplitude unstable modes, a parallel transfer process (not serial, as in damped mode to damped mode) conceivably could dominate the energetics.

To isolate the unstable and stable modes, fluctuations can be represented by either the linear eigenmode decomposition or the POD. The linear eigenmode decomposition is formed from the eigenvectors of the linear gyrokinetic operator. For numerical solutions, the operator is discretized. We make use of the gyrokinetic code GENE,²¹ which has a full eigenmode solver yielding right and left eigenvectors of the gyrokinetic operator.^{22,23} The right and left eigenvectors are orthonormal under an inner product. This is expressed as

$$\sum_{\theta, v_{\parallel}, \mu} \psi_{l, \mathbf{k}}^{(m)*}(\theta, v_{\parallel}, \mu) \psi_{r, \mathbf{k}}^{(n)}(\theta, v_{\parallel}, \mu) = \delta_{m, n}, \quad (1)$$

where $\psi_{l, \mathbf{k}}^{(m)}(\theta, v_{\parallel}, \mu)$ is the m^{th} left eigenvector, $\psi_{r, \mathbf{k}}^{(n)}(\theta, v_{\parallel}, \mu)$ is the n^{th} right eigenvector, and the sum denotes a sum over

all the grid points of θ , v_{\parallel} , and μ , with the k_x modes connected in the usual fashion by a flux tube geometry. Linear mode analyses are performed with five k_x connections to generate the extended ballooning angle. The gyrokinetic distribution function is expressed as a linear combination of the right eigenvectors

$$g_{\mathbf{k}}(\theta, v_{\parallel}, \mu, t) = \sum_n \pi_{r, \mathbf{k}}^{(n)}(t) \psi_{r, \mathbf{k}}^{(n)}(\theta, v_{\parallel}, \mu), \quad (2)$$

where $\pi_{r, \mathbf{k}}^{(n)}(t)$ is the time-dependent amplitude of the mode $\psi_{r, \mathbf{k}}^{(n)}$. In the nonlinear state $g_{\mathbf{k}}(\theta, v_{\parallel}, \mu, t)$ is governed by a balance of the linear instability, nonlinear transfer, and dissipation. However, it can always be decomposed according to Eq. (2), in which case mode amplitudes, in terms of a numerical solution of $g_{\mathbf{k}}(\theta, v_{\parallel}, \mu, t)$ are given by

$$\pi_{r, \mathbf{k}}^{(n)}(t) = \sum_{\theta, v_{\parallel}, \mu} \psi_{l, \mathbf{k}}^{(n)*}(\theta, v_{\parallel}, \mu) g_{\mathbf{k}}(\theta, v_{\parallel}, \mu, t), \quad (3)$$

where the orthonormality property of Eq. (1) has been used. Because $\psi_{r, \mathbf{k}}^{(n)}$ is an eigenvector, its corresponding complex eigenvalue, also returned by GENE's eigenmode solver, is the linear frequency and growth rate. For the CBC, there is a single unstable eigenmode. The remaining eigenmodes are all stable, with negative growth rates.

For the POD, we also have a decomposition of the gyrokinetic distribution function, given by

$$g_{\mathbf{k}}(\theta, v_{\parallel}, \mu, t) = \sum_j \hat{\beta}_{j, \mathbf{k}} \chi_{j, \mathbf{k}}(\theta, v_{\parallel}, \mu) \Theta_{j, \mathbf{k}}(t), \quad (4)$$

where $\hat{\beta}_j$ is the singular value for mode number j , and χ_j and Θ_j are the orthonormal POD modes of the spatial and temporal domains. The POD modes are not linear eigenmodes and therefore do not have a simple correspondence with linear growth rates and frequencies. Nevertheless, POD modes can be driven or damped. The rate can be determined from the POD mode-resolved energy rate of change, exclusive of nonlinear transfer

$$\gamma_j = \frac{1}{E_k(j)} \left. \frac{\partial E_k(j)}{\partial t} \right|_{N.C.}, \quad (5)$$

where

$$E_k(j) = \int dv_{\parallel} d\mu d\theta \pi n_0 T_0 |\hat{\beta}_j \chi_j|^2 / F_0 + \int d\theta D(k_{\perp}, \theta) |\phi(j)|^2 \quad (6)$$

is the conserved energy-like quantity for mode j , ϕ is the electrostatic potential, n_0 and T_0 are the background density and temperature, and D is a function of θ and k_{\perp} .¹⁸ The subscript *N.C.* indicates that this equation describes only the non-conservative energy evolution, which is governed by linear terms of the gyrokinetic equation that represent the free energy injected into the turbulence by gradients and dissipation by collisions. The energy dissipation rate of Eq. (5) is a time independent quantity, representing a steady state balance between source and sinks. Table I summarizes the nomenclature used for the two mode decompositions.

TABLE I. A table showing nomenclature for the POD and the linear eigenmode decomposition (for right eigenvectors). Both utilize a single mode number. The time dependent behavior in the functions $\Theta_{j,k}(t)$ and $\pi_{r,k}^{(n)}(t)$ reflects nonlinear dynamics.

Decomposition	Mode	Mode number	Time-dependent part (in saturation)
POD	$\chi_{j,k}(\theta, v_{\parallel}, \mu)$	j	Temporal POD mode $\Theta_{j,k}(t)$
Linear eigenmode (in right representation)	$\psi_{r,k}^{(n)}(\theta, v_{\parallel}, \mu)$	n	Time-dependent amplitude $\pi_{r,k}^{(n)}(t)$

B. Mode resolution

We now consider the relative merits of the expansions of Eqs. (2) and (4), given the limitations of finite resolution and the intrinsic differences between the decompositions. Neither is exact because they derive from a discrete representation. Well before the highest value N of n or j is reached the expansions develop noise. This can be probed by considering the mode structures of $\psi_{r,k}^{(n)}(\theta, v_{\parallel}, \mu)$ and $\chi_{j,k}(\theta, v_{\parallel}, \mu)$. Modes that are dominated by variation on the grid scale are not well resolved: because energy dissipation is most sensitive to small scale variation, such modes do not yield a reliable value for the rate of energy dissipation. In turn, because fluctuation levels depend on energy dissipation rates in a dissipation range, an energy distribution across poorly resolved modes cannot be physically meaningful. We introduce a simple metric for mode resolution to indicate where the energy distribution is meaningful.²⁴ Modes that are dominated by variation on the grid scale have large amplitude in the largest wavenumbers of a Fourier transform relative to small wavenumbers. The metric we adopt takes a Fourier transform for either the v_{\parallel} or θ variation, averaging over the remaining two phase space variables. It then takes the ratio of the average amplitude for $0 < k < k_{max}/2$ to the amplitude for $k_{max}/2 < k < k_{max}$, where k is the wavenumber of either the transform in v_{\parallel} or θ , and k_{max} is the maximum wavenumber allowed by grid resolution. When this ratio is greater than unity, the mode is considered to be well resolved. When the ratio is unity or smaller, the mode is not well resolved. We test if this metric is reasonable by comparing how it and the growth rate respond to a reduction in grid resolution from the nominal values used in the simulations described in this paper. The growth rate values are relatively unchanged and the metric shows the resolution to be adequate until the (z, v_{\parallel}) grid resolution has been reduced, separately, by more than a factor of 2. The similar responses suggest that this

metric is reasonable for assessing whether modes are resolved.

Figure 1(a) shows the ratio described in the previous paragraph as a function of POD wavenumber j , computed from the Fourier transform in θ ; Fig. 1(b) shows the ratio as a function of the linear mode number n , also from the Fourier transform in θ . Here, n labels linear modes that for $n \geq 2$ are ordered by magnitude of damping rate, with $n=2$ being the least damped mode. Both plots have scatter, but, as might be expected, there is greater scatter for the linear eigenmodes. Because the measure is crude, we do not investigate further the scatter but use centroid values to characterize the ratio as a function of wavenumber. For both plots, the ratio starts near ten and decays to unity. The two horizontal scales are different, so that while there are a few hundred well-resolved POD modes, the number of well-resolved modes for the linear eigenmode decomposition is a few thousand.

A word on the applicability of Fourier transforms in the metric of Fig. 1 is in order. In a well-resolved simulation, all relevant quantities can be expected to peak within the range of points covered by the extended ballooning angle and to fall off to very small values by the time they reach the domain boundaries. First consider this behavior, which is relevant for any well-resolved mode. Its shape becomes pseudo-periodic (as its value and that of its derivative are essentially zero at the boundary), and a Fourier transform will yield results that can be interpreted in a straightforward manner: high- k (low- k) contributions correspond to zig-zag (physical) features. Now, consider a case where the mode has significant amplitude at the boundary—a clear indication that resolution is not sufficient to properly track its structure. Here, while a Fourier transform may technically not be a suitable instrument, it still yields results corresponding to high- k features, since the centered difference stencils employed by GENE²⁵ create large derivatives at the boundaries, leading to decoupled neighboring grid points. As a consequence, physical modes require

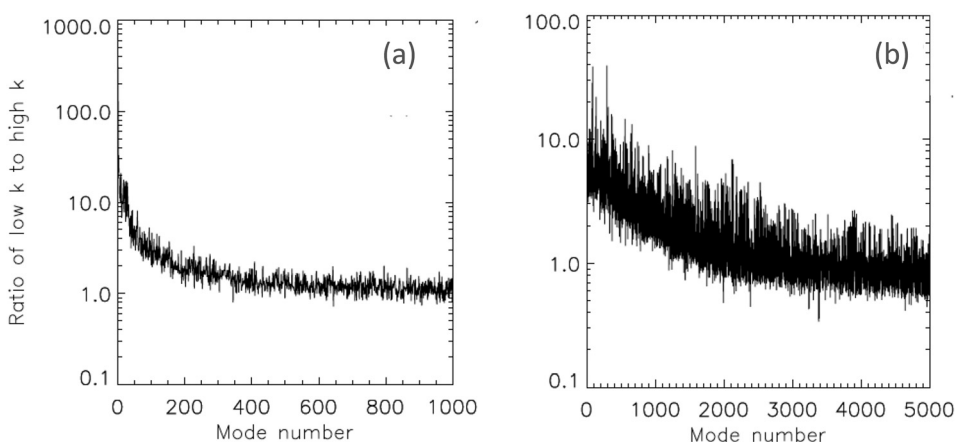


FIG. 1. Ratio of central to edge values in Fourier transforms of mode structure in the ballooning angle θ . (a) is for POD modes, (b) is for linear eigenmodes, ordered by damping rate, with $n=2$ being the least damped stable mode.

both dominantly low- k features and small boundary values— as soon as one of these conditions is no longer met, the Fourier transform and the analysis below can be expected to result in a label of “not properly resolved” for this mode.

The variation across mode numbers in Fig. 1 represents a variation in scale. This is seen in a general way in Fig. 2, which shows POD mode number j as a function of the Fourier wavenumbers for v_{\parallel} and θ , where the Fourier transform is applied to the full decomposition [Eq. (4)]. The decomposition arranges itself such that larger scales in θ and v_{\parallel} have lower j and smaller scales have higher j . To determine what range of scales is represented by modes in a mode number range $j_m < j < j_{m+n}$, we introduce the rms wavenumber of mode j

$$\langle k_{\theta} \rangle^{(j)} = \left\{ \frac{\sum_{k_{\theta}} k_{\theta}^2 |\chi_{j,k}(k_{\theta})|^2}{\sum_{k_{\theta}} |\chi_{j,k}(k_{\theta})|^2} \right\}^{1/2} \quad (7)$$

and

$$\langle k_{v_{\parallel}} \rangle^{(j)} = \left\{ \frac{\sum_{k_{v_{\parallel}}} k_{v_{\parallel}}^2 |\chi_{j,k}(k_{v_{\parallel}})|^2}{\sum_{k_{v_{\parallel}}} |\chi_{j,k}(k_{v_{\parallel}})|^2} \right\}^{1/2}, \quad (8)$$

where $\chi_{j,k}(k_{\theta})$ is the Fourier transform of $\chi_{j,k}(\theta)$, $\chi_{j,k}(k_{v_{\parallel}})$ is the Fourier transform of $\chi_{j,k}(v_{\parallel})$, and averages have been performed for the remaining variables. Root mean square wavenumbers $\langle k_{\theta} \rangle^{(n)}$ and $\langle k_{v_{\parallel}} \rangle^{(n)}$ for linear eigenmodes are defined in an analogous fashion

$$\langle k_{\theta} \rangle^{(n)} = \left\{ \frac{\sum_{k_{\theta}} k_{\theta}^2 |\psi_{r,k}^{(n)}(k_{\theta})|^2}{\sum_{k_{\theta}} |\psi_{r,k}^{(n)}(k_{\theta})|^2} \right\}^{1/2} \quad (9)$$

and

$$\langle k_{v_{\parallel}} \rangle^{(n)} = \left\{ \frac{\sum_{k_{v_{\parallel}}} k_{v_{\parallel}}^2 |\psi_{r,k}^{(n)}(k_{v_{\parallel}})|^2}{\sum_{k_{v_{\parallel}}} |\psi_{r,k}^{(n)}(k_{v_{\parallel}})|^2} \right\}^{1/2}. \quad (10)$$

We use Eqs. (7) and (8) to ascertain the wavenumber range associated with $1 < j < j_{max}$, where $j_{max} \sim 200$ is the maximum mode number for well resolved POD modes. We use Eqs. (9) and (10) to ascertain the wavenumber range associated with $1 < n < n_{max}$, where $n_{max} \sim 2000$ is the maximum mode number for well resolved linear eigenmodes. The well resolved modes of both decompositions correspond roughly to the same range of scales, a range on the order of 6. The fewer well-resolved modes of the POD reflect the optimal character of the POD in capturing the dynamics with the least number of modes. However, the larger number of linear modes allows better statistics and greater interpolative resolution of the dynamics.

The number of resolved modes depends on both the number of grid points in the discretization and the strength of dissipation.^{26,27} The latter is either collisional, or for zero collisionality, it is hyper diffusion in θ and v_{\parallel} . Figure 3 shows the amplitudes of 20 480 linear modes as a function of the mode damping rate and mode frequency for two different values of the hyperdiffusive coefficients D_{θ} and D_v .²⁵ In these simulations, collisionality is zero, and hyper diffusion provides artificial dissipation. In both cases, nonlinear observables (mode amplitude, mode energy, energy dissipation rate) are converged. No orthogonalization is performed. In (a), the diffusion coefficients are $D_{\theta} = 8.0$ and $D_v = 5.0$. The amplitudes decrease smoothly and steadily over an order-of-magnitude variation of the mode damping rate. There is no evidence of anomalous amplitude features associated with nonorthogonality. As with POD, more strongly damped modes tend to have finer structure in θ and v_{\parallel} , and the amplitude decrease ensures that a larger number of modes are well resolved. As demonstrated in Fig. 1, there are 2000–3000 well-resolved modes in the spectrum. In (b), the diffusion coefficients are much smaller, with $D_{\theta} = 0.25$ and $D_v = 0.2$. Virtually, all of the modes have very weak damping rates. A large number of weakly damped modes have fine-scale variation in θ and v_{\parallel} and large amplitudes. These are not resolved, and their amplitudes, relative to the case in (a), are anomalously high. In (b), the number of well resolved modes is order 100 only. In (a), the appearance of high-frequency modes with damping rates near 6 is an artifact of the hyper-diffusive damping. With collisional damping, high-frequency modes appear for damping rates that are

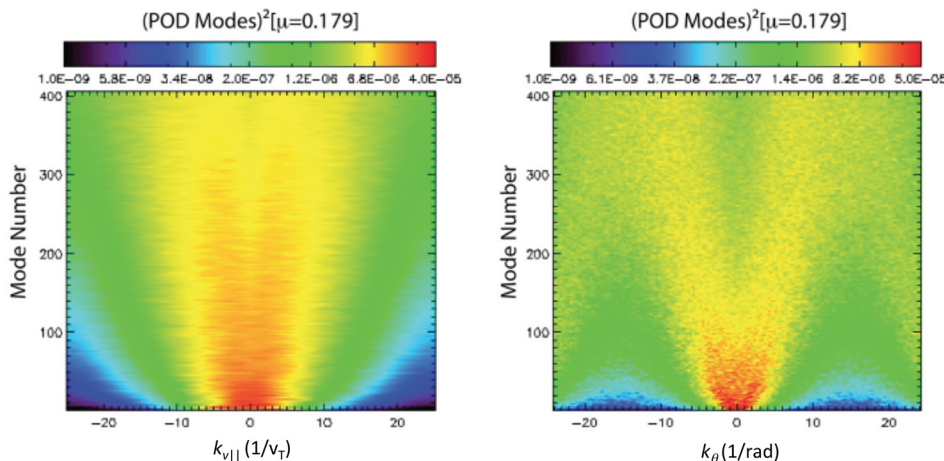


FIG. 2. Variations of POD mode number with wavenumbers for θ and v_{\parallel} .

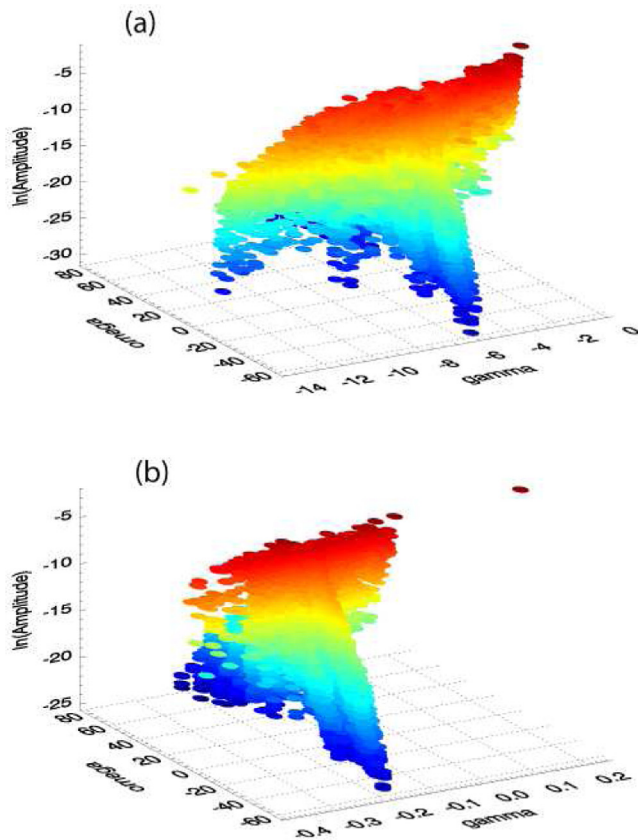


FIG. 3. Natural logarithm of time averaged linear mode amplitudes on z axis as a function of the mode damping rate (y axis) and mode frequency (x axis). For (a), the hyperdiffusivity values are $D_\theta=8.0$ and $D_v=5.0$; for (b), $D_\theta=0.25$ and $D_v=0.2$.

near zero. However, the amplitudes of the energy-containing modes, represented by high-amplitude modes along the ridge near zero frequency, fall in the category of well-resolved modes and are physically meaningful.

III. STRUCTURE OF ENERGY PATHWAY

The pathway followed by energy from mode to mode in bridging source and sink is an important consideration for the spectral distribution of energy. For example, the serial transfer of energy from scale to scale with an invariant energy dissipation rate is central to the Kolmogorov spectrum.¹ Likewise, nonlocal transfer (that jumps modes) for Prandtl number greater than unity in thermal convection yields the shallow k^{-1} spectrum of Batchelor.²⁸ Here, the fact that there are modes associated with perpendicular Fourier wavenumbers k_x and k_y , as well as the stable modes representing other degrees of freedom gives rise to additional possibilities. In fluid models of ITG turbulence, for instance, two wavenumbers of the single unstable eigenmode mode beat together to parametrically drive the stable mode.¹¹ Moreover, in fluid models, in general, the nonlinearities of each field are mixed in the linear eigenmode decomposition, so that arbitrary combinations of linear eigenmodes interact via the Fourier triplets in wavenumbers corresponding to directions of homogeneity.¹² This is supported in analyses of mode coupling in gyrokinetic ITG turbulence, where stable modes each interact with the unstable mode through the

intermediary of the zonal flow.^{15,29} Each of these latter possibilities suggest parallel pathways for energy transfer between the unstable mode and damped modes. Figure 4 shows schematic representations of a serial pathway (a), as in Kolmogorov turbulence, and a parallel pathway (b), as suggested by the examples just cited.

We devise a measurement to test the dominant energy pathway and apply it to both the POD and the linear eigenmode decomposition. For the POD, we make use of the orthogonality of $\chi_{j,k}(\theta, v_{||}, \mu)$ and extract the $j=1$ mode from $g_k(\theta, v_{||}, \mu, t)$. The $j=1$ mode is very close to the unstable mode. At one time step in the saturated phase, we increase its amplitude at wavenumber $\mathbf{k}=(0, 0.25)$ by a factor of 10, creating an impulsive energy perturbation. We then observe the transfer of the increment to coupled wavenumbers $\mathbf{k}=(0.1, 0)$ and $(-0.1, 0.25)$ for a sampling of 40 POD modes from $j=1$ to $j=352$. This choice of wavenumbers, with a zonal flow in the perpendicular wavenumber coupling between unstable and damped modes, has been shown to be the dominant energy transfer channel to damped modes in gyrokinetic models of ITG turbulence.¹⁵ Subsequent to the perturbation, the energy of damped modes undergoes a sharp rise to a maximum value well above the level of fluctuations in the steady state, after which it relaxes back, sometimes with secondary spikes within a decaying envelope. We plot in Fig. 5(c) the rise time, defined as time elapsed from the $j=1$ perturbation to the first maximum in POD modes at $\mathbf{k}-\mathbf{k}'=(-0.1, 0.25)$. Similar behavior is seen in Figs. 5(a) and 5(b) for damped modes at $\mathbf{k}=(0, 0.25)$ and $\mathbf{k}'=(0.1, 0)$. This plot indicates that over the span of 352 modes, all receive energy from the perturbed $j=1$ mode at essentially the same time.

For the linear eigenmode decomposition, we extract the unstable mode at $\mathbf{k}=(0, 0.25)$ using the orthogonality

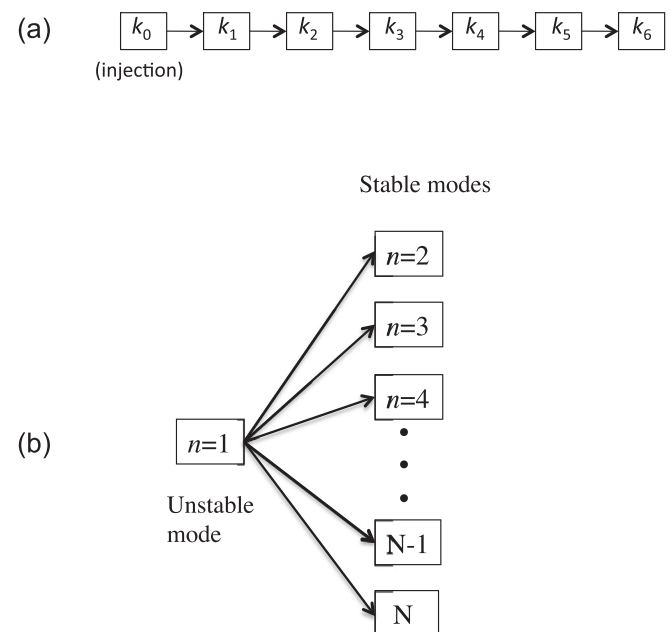


FIG. 4. A schematic of two energy pathways linking modes. (a) Represents a serial pathway typical of the wavenumber cascade of hydrodynamic turbulence. (b) Represents a parallel pathway between a single unstable mode and a collection of stable modes, all in the unstable wavenumber range.

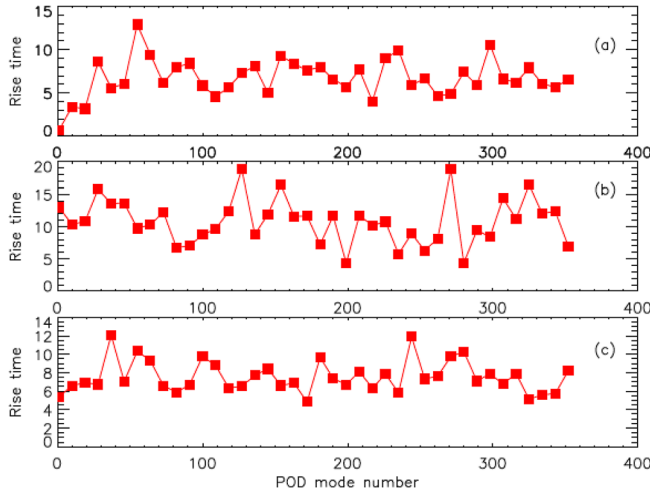


FIG. 5. Average rise time for a sample of POD modes at three wave numbers (a) $\mathbf{k} = (0, 0.25)$, (b) $\mathbf{k}' = (0.1, 0)$, and (c) $\mathbf{k} - \mathbf{k}' = (-0.1, 0.25)$. These are averaged over an ensemble of five simulation runs and plotted for a sample of 40 POD modes: 1, 10, 19, 28, ... 352.

condition of Eq. (1). An increment of 100 is applied to the amplitude. We then track the response in 5000 linear eigenmodes at the same perpendicular wavenumber \mathbf{k} . We use Eqs. (9) and (10) to convert mode number to rms wavenumbers $\langle k_\theta \rangle^{(n)}$ and $\langle k_{v_\parallel} \rangle^{(n)}$. The results are plotted in Fig. 6. Like Fig. 5, the rise times produce a very flat profile, i.e., the 5000 linear modes have a rise time that is independent of mode number. The 5000 modes represent a span of a factor of 5 in k_θ and nearly a factor of 10 in k_{v_\parallel} . As with Fig. 1, there is considerable scatter in these data. Moreover, there appear to be two rise times, one at $t \approx 0.2$ and one at $t \approx 0.8$. This may be an artifact of measuring the response in the same wavenumber as the perturbation, which requires the energy to first couple to other wavenumbers before returning to the original wavenumber. However, it remains a fact that over a significant wavenumber variation, there is no dependence of rise time on wavenumber. This contrasts with energy transfer in wavenumber space in hydrodynamic turbulence, which is local³⁰ and serial, passing through a sequence of ever smaller scales as depicted in Fig. 4(a). To see what a

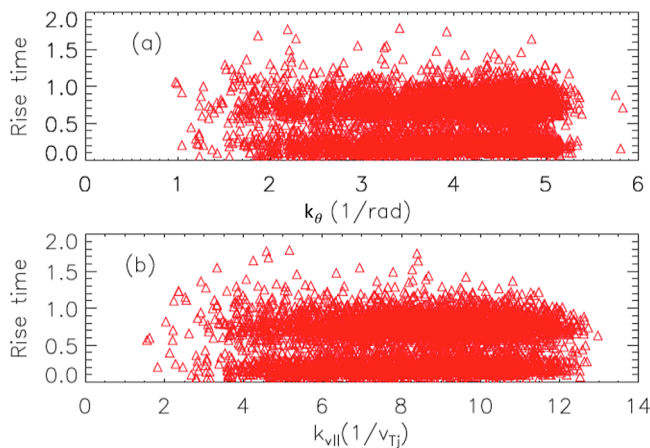


FIG. 6. Ensemble averaged rise times for the first 5000 linear modes at $\mathbf{k} = (0, 0.25)$, plotted as a function of average wavenumbers $\langle k_2 \rangle^{(n)}$ and $\langle k_{v_\parallel} \rangle^{(n)}$.

local wavenumber cascade like that of hydrodynamic turbulence looks like when subjected to a perturbation localized to some wavenumber, consider Fig. 9 of Ref. 31. There the response across the spectrum to a localized perturbation like that of Figs. 5 and 6 is measured. The system is a plasma, but the dominant nonlinearity is vorticity advection, the standard nonlinearity of hydrodynamic turbulence. Vorticity advection is associated with a forward, local-in-wavenumber cascade. In Fig. 9 of Ref. 31, the impulsive perturbation applied to a narrow band of wavenumbers is seen to spread in wavenumber space in a manner that is qualitatively diffusive. This produces later rise times for wavenumbers that are more removed from the band of the perturbation. The delay is evident between wavenumbers that differ by a factor of 3. We conclude that energy transfer in mode space for a significant number of modes is parallel rather than serial.

IV. SCALABLE REPRESENTATION OF MODE SPACE

The two mode decompositions we have analyzed have produced entirely consistent results. Both show parallel pathways for energy transfer, and the well-resolved modes of both cover comparable scale ranges. While each will yield its own energy distribution across modes space, which is used might be considered a matter of personal preference. The linear decomposition, with its considerably larger number of modes, may be better at revealing features that emerge from statistical behavior. The other consideration is whether the region of perpendicular wavenumber space we are observing is dominated more by linear physics or more by nonlinear physics. In the case of the former, the linear eigenmode decomposition is a natural choice for describing the dynamics.

We assess the importance of linear physics relative to nonlinear physics using a standard measure based on nonlinear energy transfer. Consider the dimensionless ratio

$$R = \frac{T_k}{\gamma k E(k)}, \quad (11)$$

which forms a key quantity in the dissipation of nonlinearly transferred energy.³² Here, $\gamma k E(k)$ is the net energy dissipation rate, T_k is the nonlinear spectral energy transfer rate defined below, and $E(k)$ is the 1-D spectral energy density, i.e., if kinetic energy v_k^2 were the sole component of $E(k)$, as in Navier-Stokes turbulence, we would have $E(k) = v_k^2/k$. The factor γ is the net rate at which energy is introduced into and/or removed from fluctuations at wavenumber k . For hydrodynamic turbulence in inertial and dissipation ranges, the rate γ is governed by viscous dissipation νk^2 , a linear process. In this case, R is a familiar quantity: it is the Reynolds number at the outer scale of the turbulence and is equal to unity at the Kolmogorov wavenumber k_ν .³² In the dissipation range where $k > k_\nu$, R^{-1} becomes larger than unity, increasing as $(k/k_\nu)^{2/3}$. The ratio R^{-1} thus provides a simple ratio of the single linear rate to the single nonlinear rate in isotropic hydrodynamic turbulence.

In the case under consideration in this paper, the situation is more complicated. In the wavenumber range of the instability, there is both growth through the instability

process and damping through nonlinearly excited stable modes. Consequently, γ is given by

$$\gamma = \gamma_{ITG} - \gamma_{damp}, \quad (12)$$

where γ_{ITG} is the instability growth rate and γ_{damp} is the total damping rate of damped modes at wavenumber k . For the Cyclone base case, γ_{ITG} is a single eigenvalue of the linear gyrokinetic operator. While γ_{damp} derives from the linear eigenvalues of damped modes, it is present in a stationary nonlinear state only if damped modes are nonlinearly excited. The form $\gamma_{damp}E(k)$ depends on the nonlinear amplitude of each damped mode in aggregate. Given these complexities, R^{-1} is not a simple ratio of a linear rate to a nonlinear rate, as it is in hydrodynamics.

Nevertheless, we use $R^{-1} = (\gamma_{ITG} - \gamma_{damp})kE(k)/T_k$ as a lower bound on the quantity $\gamma_{ITG}kE(k)/T_k$, which is a ratio of linear energy input rate to nonlinear transfer rate. We measure R^{-1} because it is the quantity that is most central to energy transfer, and can be extracted wholly from a single quantity T_k , whereas $\gamma_{ITG}kE(k)/T_k$ requires a series of separate measurements. Moreover, the data for finding R^{-1} from gyro kinetic simulations have already been measured and are available in Ref. 15 in a calculation based on POD.

The calculation of R^{-1} from T_k relies on the fact that spectral energy transfer suffers attenuation in wavenumber space given by (see Refs. 32 and 33)

$$\frac{dT}{dk} = \gamma E(k). \quad (13)$$

We then find from Eq. (11) that

$$\frac{k}{T} \frac{dT}{dk} = \frac{1}{R}. \quad (14)$$

The spectral energy transfer rate is $T = T(k, k')$, where

$$T(k, k') = T_{k-k', k'}^{(1)} + T_{k-k', k'}^{(S)} - (T_{k, k'}^{(1)} + T_{k, k'}^{(S)}), \quad (15)$$

and

$$T_{k, k'}^{(j)} = \text{Re} \left\{ \int dz dv_{\parallel} d\mu \frac{\pi B_0 \hat{j} n_0 T_0}{F_0} (\mathbf{k}' \times \hat{\mathbf{z}} \cdot \mathbf{k}) \times \left[\hat{\beta}_{j, \mathbf{k}} \chi_{j, \mathbf{k}}(\theta, v_{\parallel}, \mu) \Theta_{j, \mathbf{k}}(t) \right]^* (g_{k'} \bar{\phi}_{k-k'} - \bar{\phi}_{k'} g_{k-k'}) \right\}. \quad (16)$$

In Eqs. (15) and (16), the superscript (1) labels the unstable mode, (S) indicates a sum over damped modes, and the overbar indicates the gyroaverage.

In Ref. 15, the four components of $T(k, k')$ are measured in five adjacent wavenumber blocks created by varying k from (0, 0.25) to (-0.5, 0.25) in increments of $\Delta k_x = -0.1$. The wavenumber $k' = (0.1, 0.0)$ is a zonal mode whose catalysis of energy transfer provides the dominant channel from the unstable mode with $j=1$ to the stable modes with $j>1$. Differences of $T(k, k')$ between blocks provide ΔT for the derivative in Eq. (14). Figure 7 shows R^{-1} as a function of k_x constructed from the four differences between blocks. Values of $|R^{-1}|$ are bounded by ~ 0.3 and 2.8. We note that

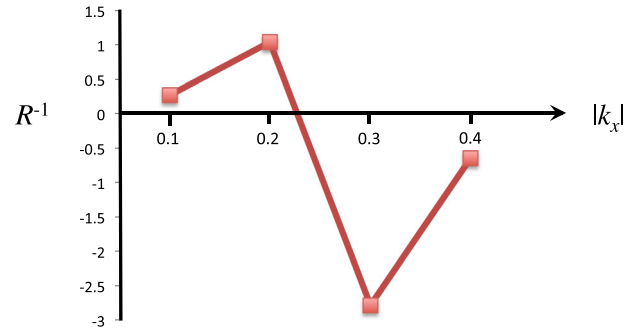


FIG. 7. Ratio of energy dissipation rate to energy transfer rate as function of perpendicular wavenumber $|k_x|$ in the saturated state of Cyclone base case ITG turbulence.

linear effects dominate when $\gamma_{ITG}kE(k)/T_k \sim O(1)$, while a dominance of nonlinear effects requires $\gamma_{ITG}kE(k)/T_k \ll 1$. The leftmost point of R^{-1} is already ~ 0.3 and therefore represents a wavenumber where linear effects are important. For the next two points at higher $|k_x|$, the lower bound already exceeds unity. Nonlinear effects dominate only when $|k_x| > 0.4$, where other analyses have shown that the system transitions to an inertial range.³² For the wavenumbers $|k_x| = 0.3$ and $|k_x| = 0.4$, the negative values of R^{-1} indicate that $\gamma_{damp} > \gamma_{ITG}$. These wavenumbers represent a regime where linear effects dominate but nonlinear physics plays an important role in making $\gamma_{damp} > \gamma_{ITG}$. On the whole, Fig. 7 indicates that the lower bound given by R^{-1} is already at or above the threshold for strong linear effects. Hence, the linear eigenmode decomposition is appropriate for representing the physics in the wavenumber range of the instability. This is particularly true because γ_{damp} has its most unequivocal determination from the linear eigenmode decomposition. We therefore choose the linear decomposition to look for a scalable representation of the distribution of energy in mode space.

In Fig. 3(a), stronger damping is correlated with smaller amplitude, which in turn is correlated with finer-scale structure in θ and v_{\parallel} , as shown in Fig. 2. There is a hint in Fig. 3(a) that a product of the damping rate and the amplitude to some power might be constant for the energy-containing modes, i.e., independent of the damping rate. These facts motivate us to treat the damping rate, which we now simply write as γ , as a label for the linear eigenmodes. More precisely, we can take discrete linear modes and number them consecutively with integers in order of increasing $|\gamma|$. With this construct, the mode number bears a relationship to scale size. Only here, where there are three independent variables θ , v_{\parallel} , and μ spanning mode space, a single mode number sorts them according to a single quantity γ . Because the mode number labels individual coupled modes, it can serve as a single abscissa that carries scaling information for the domain of coupled modes, in analogy to wavenumber in isotropic hydrodynamic turbulence. Consequently, any γ -independent product of γ and amplitude raised to some power can be reconfigured as an invariance in mode number, and potentially a property of the underlying mode coupling.

Figure 8 shows the product of γ and the amplitude squared, which we refer to as the energy dissipation rate. In the raw distribution, there is considerable scatter in the mode distributions across the thousands of modes contributing to Fig. 8. Accordingly, a running boxcar average has been applied to the figure. For mode number i , an average is done over b neighboring modes from $i - b/2$ to $i + b/2$, where b is the box size. The numbers $i - b/2$ and $i + b/2$ are rounded off to closest integers. The box size b is varied as a function of i such that the box size remains constant on a log scale. This is done by varying b proportionally to i . The exact formula used is $b = i/50$. So, for example, at mode number $i = 10$, the box size is $b = 10/50 = 0.5 \rightarrow 0$, i.e., no box averaging. At mode number $i = 100$, the box size is $b = 2$, and at mode number $i = 10\,000$, the box size is $b = 200$. This does not suppress the scatter at the lowest mode numbers but prevents an artificially constant region at low mode numbers whose width is the box size.

We observe that the energy dissipation rate is close to constant, particularly for the largest-amplitude modes, out to a mode number of ~ 1200 . The transfer pathway is parallel for the modes in this range, as depicted in Figs. 5 and 6, and we refer to the constant value of the energy dissipation rate as an equipartition. The range of equipartitioned energy dissipation rate does not extend over the entire set of well resolved modes. Hence, it is not all-encompassing. However, given the steep falloff above 1200, this range accounts for most of the energy dissipation, and therefore most of the contribution of damped modes to saturation. Above 1200, there may be a second scaling range with a power law $\gamma E \sim j^{-\alpha}$, where $\alpha \approx 3.6$. The region above 4000 where the energy dissipation rate stops falling off is a region of poorly resolved modes where the distribution cannot be regarded as physical.

If β_j is the amplitude of the j th linear eigenmode, where j is ordered by the growth rate, the equipartition of the energy dissipation rate can be expressed as

$$\gamma_j |\beta_j|^2 = \epsilon, \quad (17)$$

where $j \geq 2$ labels damped modes, γ_j is the damping rate of the j th mode, and empirically, ϵ is the constant energy

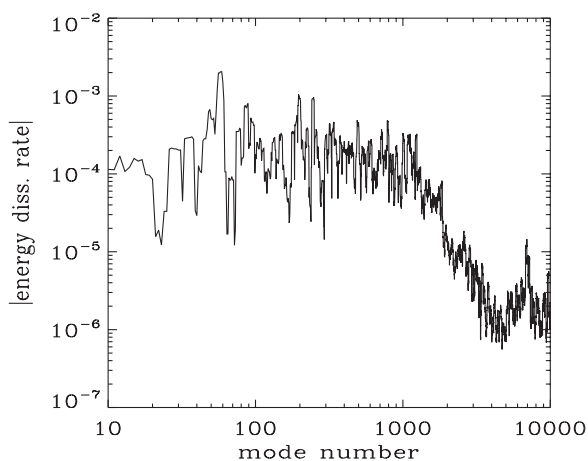


FIG. 8. Distribution of energy dissipation rate as a function of linear mode number ordered by mode damping rate.

dissipation rate of Fig. 8 in the range $j < 1200$. Because damped modes have no linear drive, ϵ is both the nonlinear energy transfer rate to the j th mode and the energy dissipation rate of the j th mode. Equation (17) is analogous to the Obukov balance of hydrodynamics, $kv^3 = \epsilon$;² only here, because energy transfer is parallel rather than serial, ϵ is the rate of energy injected by the instability in steady state divided equally among the modes receiving it simultaneously. As with hydrodynamics, Eq. (17) yields a spectrum

$$|\beta_j|^2 = \epsilon \gamma_j^{-1}, \quad (18)$$

where γ_j behaves as a scaling variable for damped modes in mode space, analogous to the role of the wavenumber.

The balance of Eq. (17) is nominally a dissipation range balance wherein nonlinear transfer is subjected to dissipative losses. As emphasized in Ref. 32, such balances apply in hydrodynamics not just at the Kolmogorov wavenumber but across all scales. Implicit in the construct is the notion that scaling behaviors of the nonlinearity remain in force in the dissipation range, even as energy is lost due to dissipation.³⁴ This has recently been verified for magnetohydrodynamics, where scale-dependent alignment, a property of the nonlinearity, was shown to extend into the dissipation range.³⁵

This allows us to argue why the system produces an equipartition of the energy dissipation rate. We postulate that the invariance of elemental energy transfer across transfer events, which is the essence of hydrodynamic turbulence,^{1,2} extends to instability-driven gyrokinetic turbulence. Since the transfer is parallel, each parallel event involves an invariant quantity of the energy dissipation rate, namely, ϵ . Since this nonlinear behavior remains in force even in a dissipation range, Eq. (17) holds.

V. DISCUSSION AND CONCLUSIONS

Stable modes that produce damping in the wavenumber range of instabilities play an important role in the saturation of instability driven plasma turbulence. The large number of such modes excited in gyrokinetic models of microturbulence raises the critical question of what governs the amplitude distribution across the space of these modes. In seeking answers to this question, we have found it necessary to examine mode decompositions and address the issue of when individual modes in a decomposition are well resolved. A metric introduced to identify well resolved modes shows that for standard resolutions in the Cyclone base ($\sim 20\,000$ grid points in the θ - v_{\parallel} - μ space spanned by damped modes), there are a few thousand well resolved linear modes and a few hundred well resolved POD modes. For both decompositions, the well resolved modes span the same scale range, which is just under a decade in θ and v_{\parallel} . There is little mode activity in μ . The difference in the number of well resolved modes for the two decompositions reflects the optimal character of the POD. An analysis of ratio of linear energy dissipation rate to the nonlinear energy transfer rate shows that linear processes dominate in the wavenumber range of the instability, indicating a particular suitability for the linear decomposition in this range.

Over the range of well-resolved linear eigenmodes, we find that the distribution of damped modes can be understood from a property of dissipation rate equipartition. Even if this property is not perfectly reflected in the spectrum, given the scatter in Fig. 8, it is a powerful idealization that links complex 5-dimensional gyrokinetic turbulence in a dissipative domain to robust and enduring principles of hydrodynamic turbulence. Present resolutions with $\sim 20\,000$ modes, while requiring significant computational resources, yield an obviously limited range of a few thousand well-resolved modes. It is clearly important to pursue simulations with very high resolution in θ , $v_{||}$, and μ in order to increase the number of well-resolved modes and see if both the constancy of rise times (Figs. 5 and 6) and energy dissipation rate equipartition extend to larger numbers of modes. We note that the equipartition of dissipation rate has been demonstrated with a linear mode decomposition that is not orthogonalized. Given the smooth falloff of the spectrum and the demonstration that modes are well resolved, we do not expect that orthogonalization will significantly change the results. However, that remains to be shown.

At this point, we do not have the information at hand to know whether the equipartition range in mode number n applies to all well-resolved modes or a subset, albeit a significant subset. Answering that question will require additional analysis, either from simulations with considerably higher resolution or from some form of analytic theory. In any case, given the falloff in Fig. 8 above n of a few thousand, modes in the equipartition range dominate the energy dissipation rate and therefore govern the contribution of damped modes to saturation. Note that, because modes with higher n have a larger damping rate, making amplitudes successively weaker, modes in the lower mode number part of the equipartition range also dominate the energy. This means that the equipartition range with its simple analytic scaling law of Eq. (18) characterizes the spectrum of energy-containing and transport-governing modes. As such, these laws should be sufficient for deriving saturation rules that account for the dissipation of the damped-mode spectrum and for creating simple but widely applicable transport models.

We expect that these results are applicable to a wide range of turbulent systems driven by plasma microinstability. The results presented here are specific to Cyclone base-case ITG turbulence for experimentally relevant collisionalities.⁹ ITG turbulence is a major cause of ion-channel heat loss in tokamaks. While the Cyclone base case has a single unstable mode, our results are readily adapted to cases with multiple unstable modes by taking ϵ as the energy injection rate averaged over the unstable modes. Tokamaks are susceptible to, and experience losses from other instabilities, in particular, trapped electron mode (TEM) instability,^{37,38} and in the case of spherical tokamaks, microtearing instability.^{39,40} Damped modes have been shown to provide saturation in both of these systems, albeit from analysis with fluid models.¹² In TEM, the excitation and effect of damped modes in saturation is similar to ITG, provided the system is in the weakly collisional limit where electron collision frequency is less than the diamagnetic frequency. In general, damped modes are expected to play a role in many types of

instability-driven plasma turbulence systems. It is required that there be damped modes for which the damping rate is not significantly larger than the growth rate, and that the nonlinearity not somehow excludes transfer to damped modes. Nonlinearities rarely exclude transfer to damped modes, and the former is generally satisfied for drift-type instabilities.

Beyond the practical matters of saturation rules and transport models, the scaling range of energy transfer in the inhomogeneous mode space of gyrokinetic turbulence, which emerges when a single integer mode number is ordered by the linear damping rate γ , is indicative of fundamental nonlinear behavior. The scaling relies on the use of γ as a scale variable, and on the independence of the energy transfer rate with respect to mode number. The latter is associated with transfer from the unstable mode that drives damped modes directly and simultaneously, in a process that is parallel rather than serial. In addition to providing a scaling relation for the energy distribution in mode space, Eq. (18), these results have two other significant implications. (1) The invariance of energy dissipation rate in hydrodynamic turbulence applies to the novel parallel transfer in the gyrokinetic mode space. In the former, the transfer is serial and the energy transfer rate is the same in each scale, including the Kolmogorov scale where the energy is dissipated; in the latter, the energy transfer process is parallel, requiring that the total energy transferred in a nonlinear time scale be equally divided among modes. The invariance establishes branching laws whose application to the parallel and serial arrangements is like the Kirchhoff laws of parallel and serial circuits. (2) Cascade properties attributed to nonlinear invariance survive in dissipation ranges. For serial transfer, the cascade proceeds in all scales according to $dT/dk = \gamma E$, where dT/dk is the attenuation of spectral transfer rate, γ is the damping rate, and E is the spectral energy density.³² For parallel transfer, the subdivided energy transfer rate is dissipated by each damped mode at its rate, $\epsilon = \gamma_j |\beta_j|^2$.

The equipartitioned distribution and invariance of energy dissipation rate and the resulting scaling behavior with γ_j apply only to the linear eigenmode decomposition. While a distribution law for the POD can readily be constructed from numerical solutions, it is not straightforward to understand it because it has not been possible to tie any distribution trend to a physically meaningful property, at least in a transparent fashion. It is not surprising that scaling properties differ from one decomposition to another, given that one decomposition effectively constructs its basic modes from linear combinations of modes of the other. The defining characteristic of POD, the maximization of the energy contained in any level of truncation, provides a conceptual mapping to the most energetic structures. However, it is not clear how this property relates to energy transfer rates, which govern the steady state.

There are reasons why the linear eigenmode decomposition is more appropriate for expressing symmetry and order in mode-space nonlinear transfer in the unstable perpendicular wavenumber range. As demonstrated in Fig. 7, linear physics is strong in this range. While linear eigenmodes are modified by nonlinearity, they still retain important features.

A second important feature is the mode frequency, which has a strong effect on energy transfer rates in weak turbulence regimes where linear rates dominate. The frequencies of turbulence at fixed wavenumber are very close to linear mode frequencies in the instability wavenumber range, thereby establishing a weak turbulence regime. In a study of this effect for Hasegawa-Wakatani turbulence, the only non-linear effect in this regime was a shift of the linear frequency.³⁶ The frequency spectrum remained highly peaked, i.e., there was no broadening of the line width. This is critical because the three-wave frequency mismatch $\omega(k) + \omega(k') + \omega(k - k')$ for coupled Fourier wavenumbers k , k' , and $k - k'$ is important for mediating the rate of nonlinear energy transfer. Unbroadened frequencies allow direct coupling between the unstable mode and damped modes. Broadened frequencies, on the other hand, are characteristic of multiple mode coupling paths and back-and-forth energy exchanges, both of which legislate against the notions on which energy dissipation rate equipartition rests. We speculate that the equipartition range of Fig. 6 persists only in a weak turbulence regime associated with lower j . Above some critical j , mode frequencies will broaden as they do for larger perpendicular wavenumbers, and energy dissipation rate will vary with j . This may explain the break in Fig. 6 above $j = 1200$ and will be investigated in future work.

ACKNOWLEDGMENTS

The authors acknowledge useful input from Greg Lau. This material is based on the work supported by the U.S. Department of Energy, Office of Science, Fusion Energy Sciences, under Award No. DE-FG02-89ER53291.

¹A. N. Kolmogorov, Dokl. Akad. Nauk. SSSR **30**, 299 (1941).

²A. M. Oboukhov, Isv. Geogr. Geophys. Ser. **13**, 58 (1949).

³S. Y. Chen, B. Dhruva, S. Kurien, K. R. Sreenivasan, and M. A. Taylor, *J. Fluid Mech.* **533**, 183 (2005).

⁴B. A. Carreras, L. Garcia, and P. H. Diamond, *Phys. Fluids* **30**, 1388 (1987).

⁵D. R. Hatch, P. W. Terry, F. Jenko, F. Merz, and W. M. Nevins, *Phys. Rev. Lett.* **106**, 115003 (2011).

⁶M. A. Beer, S. C. Cowley, and G. W. Hammett, *Phys. Plasmas* **2**, 2687 (1995).

⁷A. Bañón Navarro, P. Morel, M. Albrecht-Marc, D. Carati, F. Merz, T. Görler, and F. Jenko, *Phys. Rev. Lett.* **106**, 055001 (2011).

⁸J. Candy, R. E. Waltz, and M. N. Rosenbluth, *Phys. Plasmas* **11**, 1879 (2004).

⁹D. R. Hatch, F. Jenko, A. Navarro, and V. Bratanov, *Phys. Rev. Lett.* **111**, 175001 (2013).

¹⁰D. R. Hatch, F. Jenko, V. Bratanov, and A. Bañón Navarro, *J. Plasma Phys.* **80**, 531 (2014).

¹¹P. W. Terry, D. A. Baver, and S. Gupta, *Phys. Plasmas* **13**, 022307 (2006).

¹²K. Makwana, P. W. Terry, J.-H. Kim, and D. R. Hatch, *Phys. Plasmas* **18**, 012302 (2011).

¹³J.-H. Kim and P. W. Terry, *Phys. Plasmas* **17**, 112306 (2010).

¹⁴D. R. Hatch, P. W. Terry, F. Jenko, F. Merz, M. J. Pueschel, W. M. Nevins, and E. Tang, *Phys. Plasmas* **18**, 055706 (2011).

¹⁵K. Makwana, P. W. Terry, M. J. Pueschel, and D. R. Hatch, *Phys. Rev. Lett.* **112**, 095002 (2014).

¹⁶W. Horton, *Rev. Mod. Phys.* **71**, 735 (1999).

¹⁷G. Berkooz, P. Holmes, and J. L. Lumley, *Annu. Rev. Fluid Mech.* **25**, 539 (1993).

¹⁸D. R. Hatch, "Mode analyses of gyrokinetic simulations of plasma micro-turbulence," Ph.D. dissertation (University of Wisconsin-Madison, 2010), p. 32.

¹⁹J. A. Krommes, *Annu. Rev. Fluid Mech.* **44**, 175 (2012).

²⁰A. M. Dimits, G. Bateman, M. A. Beer, B. I. Cohen, W. Dorland, G. W. Hammett, C. Kim, J. E. Kinsey, M. Kotschenreuther, A. H. Kritz, L. L. Lao, J. Mandrekas, W. M. Nevins, S. E. Parker, A. J. Redd, D. E. Schumaker, R. Sydora, and J. Weiland, *Phys. Plasmas* **7**, 969 (2000).

²¹F. Jenko, W. Dorland, M. Kotschenreuther, and B. N. Rogers, *Phys. Plasmas* **7**, 1904 (2000).

²²M. Kammerer, F. Merz, and F. Jenko, *Phys. Plasmas* **15**, 052102 (2008).

²³F. Merz, C. Kowitz, E. Romero, J. E. Roman, and F. Jenko, *Comput. Phys. Commun.* **183**, 922 (2012).

²⁴K. D. Makwana, "Damped modes in plasma microturbulence: saturation, regulation, and energy partition," Ph.D. dissertation (University of Wisconsin-Madison, 2013).

²⁵M. J. Pueschel, T. Dannert, and F. Jenko, *Comput. Phys. Commun.* **181**, 1428 (2010).

²⁶V. Bratanov, F. Jenko, D. R. Hatch, and S. Brunner, *Phys. Plasmas* **20**, 022108 (2013).

²⁷P. P. Hilscher, K. Imadera, J. Q. Li, and Y. Kishimoto, *Phys. Plasmas* **20**, 082127 (2013).

²⁸G. K. Batchelor, *J. Fluid Mech.* **5**, 113 (1959).

²⁹D. R. Hatch, M. J. Pueschel, F. Jenko, W. M. Nevins, P. W. Terry, and H. Doerk, *Phys. Rev. Lett.* **108**, 235002 (2012).

³⁰R. H. Kraichnan, *J. Fluid Mech.* **47**, part 3, 525 (1971).

³¹D. E. Newman, P. W. Terry, P. H. Diamond, and Y.-M. Liang, *Phys. Fluids B* **5**, 1140 (1993).

³²P. W. Terry, A. F. Almagri, G. Fiksel, C. B. Forest, D. R. Hatch, F. Jenko, M. D. Nornber, S. C. Prager, K. Rahbarnia, Y. Ren, and J. S. Sarff, *Phys. Plasmas* **19**, 055906 (2012).

³³H. Tennekes and J. L. Lumley, *A First Course in Turbulence* (MIT, Cambridge, 1972).

³⁴P. W. Terry and V. Tangri, *Phys. Plasmas* **16**, 082305 (2009).

³⁵J. Mason, F. Cattaneo, and S. Boldyrev, *Phys. Plasmas* **19**, 055902 (2012).

³⁶J. Kim and P. W. Terry, *Phys. Plasmas* **20**, 102303 (2013).

³⁷D. R. Ernst, P. T. Bonoli, P. J. Catto, W. Dorland, C. L. Fiore, R. S. Granetz, M. Greenwald, A. E. Hubbard, M. Porkolab, M. H. Redi, J. E. Rice, and K. Zhurovich, *Phys. Plasmas* **11**, 2637 (2004).

³⁸T. Dannert and F. Jenko, *Phys. Plasmas* **12**, 072309 (2005).

³⁹W. Gutfenfelder, J. L. Peterson, J. Candy, S. M. Kaye, Y. Ren, R. E. Bell, G. W. Hammett, B. P. LeBlanc, D. R. Mikkelsen, W. M. Nevins, and H. Yuh, *Nucl. Fusion* **53**, 093022 (2013).

⁴⁰H. Doerk, F. Jenko, M. J. Pueschel, and D. R. Hatch, *Phys. Rev. Lett.* **106**, 155003 (2011).